Title
Cardiac PET perfusion tracers: current status and future directions.

Journal
Seminars in nuclear medicine, 44(5)

ISSN
0001-2998

Authors
Maddahi, Jamshid
Packard, René RS

Publication Date
2014-09-01

DOI
10.1053/j.semnuclmed.2014.06.011

Peer reviewed

Published in final edited form as:
Semin Nucl Med. 2014 September ; 44(5): 333–343. doi:10.1053/j.semnuclmed.2014.06.011.

Cardiac PET Perfusion Tracers: Current Status and Future Directions

Jamshid Maddahi, MD, FACC, FASNC[1,2] and **René R. S. Packard, MD**[1]

[1]Department of Medicine (Cardiology), Ronald Reagan UCLA Medical Center, University of California at Los Angeles (UCLA) School of Medicine, Los Angeles, California

[2]Department of Molecular and Medical Pharmacology (Nuclear Medicine), Ronald Reagan UCLA Medical Center, University of California at Los Angeles (UCLA) School of Medicine, Los Angeles, California

Abstract

Positron emission tomography (PET) myocardial perfusion imaging (MPI) is increasingly used for non-invasive detection and evaluation of coronary artery disease (CAD). However, the widespread use of PET MPI has been limited by shortcomings of the current PET perfusion tracers. Availability of these tracers is limited by need for an on-site (^{15}O water and ^{13}N ammonia) or nearby (^{13}N ammonia) cyclotron or commitment to costly generators (^{82}Rb). Due to short half-lives ranging from 76sec for ^{82}Rb, to 2.1min for ^{15}O water and 10min for ^{13}N ammonia, their use in conjunction with treadmill exercise stress testing is either not possible (^{82}Rb and ^{15}O water) or is not practical (^{13}N ammonia). Furthermore, the long positron range of ^{82}Rb makes image resolution suboptimal and its low extraction limits its defect resolution.

In recent years, development of an ^{18}F labeled PET perfusion tracer has gathered considerable interest. The longer half-life of ^{18}F (108 minutes) would make the tracer available as a unit dose from regional cyclotrons and allow use in conjunction with treadmill exercise testing. Furthermore, the short positron range of ^{18}F would result in better image resolution. ^{18}F flurpiridaz is by far the most thoroughly studied in animal models, and is the only F18-based PET MPI radiotracer currently undergoing clinical evaluation. Pre-clinical and clinical experience with ^{18}F flurpiridaz demonstrated a high myocardial extraction fraction, high image and defect resolution, high myocardial uptake, slow myocardial clearance, and high myocardial-to-background contrast which was stable over time – important properties of an ideal PET MPI radiotracer. Pre-clinical data from other ^{18}F labeled myocardial perfusion tracers are encouraging.

Introduction

Currently, single photon emission computed tomography (SPECT) myocardial perfusion imaging (MPI) remains the mainstay of risk stratification of coronary artery disease (CAD).

Corresponding author: Jamshid Maddahi, MD, FACC, FASNC, Professor of Molecular and Medical Pharmacology (Nuclear Medicine) and Medicine (Cardiology)., David Geffen School of medicine at UCLA, 100 Medical Plaza, Suite 410, Los Angeles, CA 90095., Phone: 310-824-4991, jmaddahi@mednet.ucla.edu.

Disclosure: Dr. Maddahi is the lead Principal Investigator for ^{18}F flurpiridaz Phase I, II and III clinical trials, chair of the steering committee and a scientific advisor to Lantheus Medical Imaging.

However, several factors affect the accuracy of this test, in particular uncorrected non-uniform attenuation and photon scatter from extra-cardiac sources, particularly the liver. Attenuation artifacts are frequently observed due to the diaphragm as well as in obese patients and female patients. Positron emission tomography (PET) cardiac imaging has inherent attenuation correction and has superior spatial and temporal resolution compared to SPECT. This has led to the growing use of PET MPI in clinical practice. However, several limitations of the currently available PET perfusion tracers have hampered their widespread use. The short half-life of these tracers necessitates either the availability of an on-site cyclotron or costly generators. This has also rendered exercise treadmill testing impractical in routine streamlined clinical practice. Ensuingly, academic and biotechnology industry researchers over the last decade exhibited a growing interest in the development of an ^{18}F-based radiotracer in an effort to take advantage of the much longer 108min half-life of ^{18}F. This has led to a sharp growth in recent years in the development and experimental animal testing of ^{18}F-based PET MPI radiotracers (1) (2) (3). The present article will review currently available PET MPI tracers and will revisit some of the more thoroughly studied ^{18}F-based radiotracers at the basic and translational level.

Current myocardial perfusion PET tracers

Three PET myocardial perfusion tracers are currently available for clinical use: ^{15}O water, ^{13}N ammonia, and ^{82}Rubidium. These tracers are different from one another with respect to their myocardial uptake, myocardial extraction fraction, positron range, half-life, production and use in the clinical setting, points that are discussed below.

^{15}O water

Myocardial uptake of ^{15}O water is through passive diffusion (4). The physical half-life of this tracer is 2.06 minutes (5). As such its production requires an on-site cyclotron (Table 1).

Image resolution of PET tracers depends on their positron energy. Tracers that emit a higher energy positron have a lower image resolution because their high energy positron travels a longer distance away from the organ before they annihilate. In other words, the higher the energy of the emitted positron, the longer the positron range and the lower the image resolution (Figure 1). ^{15}O has a 4.14 mm positron range (5) resulting in an intermediate image resolution (Figure 1).

Perfusion defect contrast is influenced by the myocardial extraction fraction of the myocardial perfusion tracer that is used for imaging. Figure 2 illustrates conceptually the relationship between myocardial blood flow (x-axes) and myocardial tracer uptake (y-axes) at baseline and at peak hyperemia. In these examples, myocardial blood flow (MBF) in a region supplied by a normal coronary artery increases to 2.4 ml/min/g, while in the region subtended by a moderately narrowed coronary artery it increases to only 1.8 ml/min/g (25% less than the normal region). The myocardial extraction fraction of ^{15}O water is 100% (6). When this tracer is used for imaging, the difference in myocardial tracer uptake would be directly proportional to the difference in flow. In other words, tracer uptake in the under-perfused region would be 25% lower than that in the normal region (estimated 1.8 versus

2.4) (Figure 2A). Nevertheless, myocardial perfusion image quality with ^{15}O water is suboptimal due to a low myocardial-to-background count ratio.

Due to its very short half-life, stress imaging with ^{15}O water is only feasible in conjunction with pharmacologic stress, not treadmill exercise. The imaging protocol consists of injection of 24-30 mCi (900-1100 MBq) of the tracer at rest followed by dynamic imaging for 4-5min (14×5sec, 3×10sec, 3×20sec, and 4×30sec) (7). Pharmacological stressor administration may begin shortly after completion of rest image acquisition, due to the short half-life of ^{15}O water. Again, 24-30 mCi (900-1100 MBq) of the tracer is injected, this time at peak hyperemia, followed by dynamic imaging for 4-5min (7).

^{15}O water has been validated and extensively used for quantitation of MBF and coronary flow reserve (CFR) (4) (6) (8) (9). However, ^{15}O water is not approved by the FDA for clinical use and is not reimbursed by third party payers. The current clinical use of ^{15}O water is primarily for measuring MBF in research studies and in the academic setting.

^{13}N ammonia

This tracer is taken up by the myocardium by passive free diffusion across cell membranes as ammonia (NH_3) where it equilibrates with its charged form ammonium (NH_4) and gets trapped inside the cell by conversion through glutamine synthase to ^{13}N-glutamine (10) (11) (12). The physical half-life of ^{13}N ammonia is 9.96 minutes (5). As such, its production has required an on-site cyclotron (Table 1). Due to the 9.96 minute half-life of ^{13}N ammonia, production and delivery of this tracer from a cyclotron a few miles away has been shown to be feasible. More recently, small, single site ^{13}N ammonia cyclotrons have been developed *(Ionetix)* that allow on-site production and unit dose use of ^{13}N ammonia in the clinical setting. However research reports with this product are lacking at present. The positron range of ^{13}N ammonia is 2.53 mm (5) resulting in an intermediate-high image resolution as compared to other PET MPI tracers (Figure 1). The myocardial extraction fraction of ^{13}N ammonia is is approximately 80% (Table 1). Therefore, there is less difference in tracer uptake in the under-perfused versus normally perfused regions as compared to ^{15}O water (Figure 2B). In other words the under-perfused to normal hyperemic blood flow ratio of 0.75 (1.8/2.4) would result in a tracer uptake ratio of 0.84 (1.3/1.55). Therefore, tracer uptake in the under-perfused region would be 16% below that of the normal region.

Since the physical half-life of ^{13}N ammonia is longer than those of ^{15}O water and ^{82}Rb, it is feasible to use ^{13}N ammonia in conjunction with supine bicycle exercise (13) (14) or treadmill exercise (15). This approach, however, is not practical for routine clinical use. ^{13}N ammonia has been validated and extensively used for quantitation of MBF and coronary flow reserve in a variety of clinical conditions with a standard clinical protocol involving injection of 20 mCi (740 MBq) of ^{13}N ammonia at rest followed by a 10min image acquisition protocol, 30min after which a pharmacological stress is performed and a second 20 mCi (740 MBq) injection of ^{13}N ammonia performed and images acquired (16) (17) (18) (19) (20) (9). This tracer is approved by the FDA for clinical use and is reimbursed by third party payers.

^{82}Rb

This tracer is taken up by the myocardium as a potassium analog through active transport by the Na^+/K^+ ATPase-pump (21) (22) (23). The physical half-life of ^{82}Rb is 1.25 minutes (5) and can be produced by a relatively small on-site generator (Table 1). Availability of ^{82}Rb generators have been hampered by limited availability of ^{82}Sr and a single supplier for ^{82}Rb generators. Recently however, a new ^{82}Rb generator delivery system has been developed, comprised of a ^{82}Sr/^{82}Rb generator and an elution system that may offer improvement in safety (Jubilant/DraxImage). *This system is available in Canada and is currently under review by the US FDA.* The positron range of ^{82}Rb is 8.6 mm (5) resulting in low image resolution as compared to other PET MPI tracers (Figure 1). The myocardial extraction fraction of ^{82}Rb is lower than the other PET perfusion tracers (Table 1). Therefore, there is less difference in tracer uptake in the under-perfused versus normally perfused regions (Figure 2C): the same stress response would result in tracer uptake of 1.0 in the normally perfused bed and 0.9 in the bed served by the stenotic vessel. Therefore, tracer uptake in the under-perfused region would be only 10% below that of the normal region.

The clinical imaging protocol for ^{82}Rb starts with initial scout and transmission CT scans obtained for orientation and attenuation correction. Beginning with the intravenous bolus administration of 50 mCi (1850 MBq) of ^{82}Rb, serial dynamic images are acquired for 6 min (14×5sec, 6×10sec, 3×20sec, 3×30sec and 1×90sec). Rapidly after completion of the rest study, a standard intravenous vasodilator infusion is administered. At peak hyperemia, a second 50 mCi (1850 MBq) dose of ^{82}Rb is injected, and images recorded in the same manner (24) (25). Although the low myocardial extraction fraction of ^{82}Rb does not render it ideal for absolute quantitation of MBF and CFR, this tracer has been extensively validated for this purpose (23) (26) (27) (28) and has provided useful information in the clinical setting (29) (30) (31) (32)

Future directions

Over the past few years, several ^{18}F labeled myocardial perfusion PET tracers have been developed. Among these tracers, ^{18}F flurpiridaz, formerly BMS-747158 or 2-tert-butyl-4-chloro-5-[4-(2-(^{18}F)fluoroethoxymethyl)-benzyloxy]-2H-pyridazin-3-1, has entered phase 3 multicenter clinical trials and will be discussed in more detail. Data on other new ^{18}F labeled tracers that are in pre-clinical investigation, such as fluorodihydrorotenone (F18-FDHR), p-fluorobenzyl triphenyl phosphonium cation (F18-FBnTP) and 4-fluorophenyl triphenyl phosphonium ion (F18-FTPP), will also be reviewed. Additional novel ^{18}F labeled PET MPI radiotracers based on various iterations of triphenyl phosphonium salts are currently being studied (33), (34), (35), (36). Given these are mostly at preliminary stages of development, they will not be discussed below.

^{18}F flurpiridaz

^{18}F flurpiridaz is a novel PET MPI tracer which is a structural analog of the insecticide pyridaben, a known inhibitor of the NADH:ubiquinone oxidoreductase also known as mitochondrial complex-1 (MC-1) of the electron transport chain (37). Flurpiridaz inhibits MC-1 by competing for binding with ubiquinone without affecting the viability of

cardiomyocytes. Uptake and washout kinetics of Flurpiridaz in rat cardiomyocytes demonstrated a very rapid uptake with a time to ½-maximal uptake of 35sec, and slow washout with an efflux ½-time greater than 120min. *In vivo* biodistribution studies in mice demonstrated that Flurpiridaz had the highest accumulation in the heart, with a substantial myocardial uptake of 9.5% injected dose per gram at 60min with very favorable heart-lung and heart-liver ratios of 14.1 and 8.3, respectively (37). Mouse microPET images acquired from 5-15min and from 55-65min demonstrated clear visualization of the left ventricular myocardium with minimal background activity. Importantly, cardiomyocyte toxicity was not observed when cells were incubated for 18h at concentrations up to 1umol/L. Importantly, the highest concentration of Flurpiridaz used in studies did not exceed 200 nmol/L with a maximal incubation time of 45min, permitting to safely conclude that cardiomyocyte viability is not affected.

Further experimental PET imaging in rats, rabbits and rhesus monkeys demonstrated a high and sustained cardiac uptake which was proportional to blood flow (38). In rats, heart-lung ratio was 9.5 at 15min with ^{18}F flurpiridaz compared to 2.0 with ^{99m}Tc sestamibi, whereas heart-liver ratio was 2.6 at 15min with ^{18}F flurpiridaz compared to 1.9 for ^{99m}Tc sestamibi. Ratios at 60min were also more favorable to ^{18}F flurpiridaz. In isolated rabbit hearts, the net ^{18}F flurpiridaz uptake increased proportionally at blood flow rates of 1.66 – 5.06 mL/min/g of left ventricular weight, achieving a slope of 0.47. In comparison, ^{201}Tl and ^{99m}Tc sestamibi achieved a slope of 0.10 and 0.08, respectively. MicroPET images acquired in rats, rabbits and rhesus monkeys from 5-15min and from 55-65min demonstrated clear visualization of the myocardium with negligible background activity. Percent change in tracer activity in the heart was determined in 5 rhesus monkeys at 10min intervals following the initial injection, with essentially constant levels in the heart after 60min. The left coronary was ligated in rat hearts to visualize myocardial perfusion deficits with blue dye injection used as the reference. The no-flow region by PET matched the one with absence of dye histologically. In a pig model, ^{18}F flurpiridaz exhibits significantly higher activity ratios of the myocardium vs. the blood, liver and lungs compared to ^{13}N ammonia (39). A small increase in myocardial tracer uptake was noted from 10–40min, both at rest and adenosine stress, suggesting the presence of tracer metabolites.

Finally, this radiotracer also permits evaluation of myocardial infarction (MI) size in rats (40). Left coronary arteries were ligated either permanently – inducing transmural MI's - or transiently for 30min – inducing subendocardial MI's - and triphenyltetrazolium chloride staining of tissue samples used as a reference of infarct size. The animals were imaged 24h thereafter. There was an excellent correlation of the defect size by microPET imaging with the MI size both after permanent (r=0.88) and transient (r=0.92) LAD ligation.

Imaging characteristics and potential clinical advantages of ^{18}F flurpiridaz are described below:

Unit dose availability—^{18}F flurpiridaz has a half-life of 108 minutes and may be produced at regional cyclotrons and delivered to imaging centers in much the same way as ^{18}F-labeled fluorodeoxyglucose (FDG), thus obviating the need for an on-site cyclotron (Table 1).

High image resolution—The positron range of ^{18}F is 1.03 mm and is shorter than those of ^{82}Rb (8.6 mm), $H_2{}^{15}O$ (4.14 mm), and $^{13}NH_3$ (2.53 mm) (5) (Table 1 and Figure 1). Image resolution of ^{18}F flurpiridaz PET is also better than ^{99m}Tc SPECT. It is expected that improved image resolution leads to improved image quality and confidence of interpretation. In Phase II clinical trials (41), image qualities of rest and stress images obtained by ^{18}F flurpiridaz PET and ^{99m}Tc SPECT were compared by blinded observers in the same patients undergoing both studies. A higher percentage of images were rated as excellent/good by PET versus SPECT on stress (99.2% vs. 88.5%, $p < 0.01$) and rest (96.9% vs. 66.4, $p < 0.01$) images. Diagnostic certainty of interpretation (define as percentage of cases with definitely abnormal/normal interpretation) was higher for PET versus SPECT (90.8% vs. 70.9%, $p < 0.01$).

High extraction fraction and perfusion defect resolution—The first-pass extraction fraction of ^{18}F flurpiridaz by the myocardium was determined in isolated rat hearts perfused with the Langendorff method (42). The radiotracer demonstrated an elevated – 94% – and flow-independent extraction fraction of ^{18}F flurpiridaz, implying a linear relationship between uptake and MBF, an important attribute for stress MBF measurements. In comparison, ^{13}N ammonia has an extraction fraction of 82% at rest and ^{82}Rb chloride one of 42% with a significant roll-off phenomenon, i.e. low extraction at high flows. The 94% extraction fraction of ^{18}F flurpiridaz did not change significantly at flows ranging from 5.0 – 16.6 mL/min which were achieved using adenosine stress. This is a result of the high density of mitochondria in cardiac muscle (which comprise 20-30% of the myocardial intracellular volume) doubled by the lipophilicity of the compound and its high binding affinity to MC-1 (38). The primary route of excretion of the compound is renal, consistent with a rapid decrease in activity of the radiotracer in the kidneys. Higher myocardial extraction facilitates detection of milder perfusion defects, as shown in Figure 2 (43). With a high-extraction radiotracer such as flurpiridaz, a substantial difference in tracer uptake is expected in normal versus under-perfused regions. With the same stress response illustrated in Figure 2D (MBF increases to 2.4 ml/min/g in the normal vascular bed and to 1.8 ml/min/g in the bed served by the stenotic vessel), tracer uptake is estimated to be 2.0 and 1.6, respectively. Therefore, tracer uptake in the under-perfused region would be 20% below that of the normal region (Figure 2D). In Phase 2 clinical trials, the magnitude of reversible defects was greater with PET than SPECT ($p = 0.008$) in patients who had CAD on invasive coronary angiography.

Low radiation exposure—In Study 101 (44), the mean effective dose (ED) of ^{18}F flurpiridaz injected at rest was very similar to that of FDG, with a much lower exposure to the critical organ by a factor of 2.5. In Study 102 (45), dosimetry of ^{18}F flurpiridaz was evaluated in patients who were injected at rest and on a second day, at peak adenosine stress or at peak treadmill exercise. Excellent image quality was noted with both forms of stress imaging. Dosimetry results suggest that injection of up to 14 mCi (518 MBq) of ^{18}F flurpiridaz during a rest-stress protocol would provide a clinically acceptable ED at 6.4 mSv. This is significantly lower than ED's of stress-redistribution ^{201}Tl imaging (26 mSv) and rest-stress ^{99m}Tc SPECT imaging (11.5 mSv). ^{18}F flurpiridaz radiation exposure is 6.3 mSv, which is approximately one half of ^{99m}Tc SPECT MPI and is similar to that of ^{82}Rb 3D imaging (4.3 mSv).

Feasibility of rest-treadmill exercise imaging—The longer half-life of ^{18}F also ensures that the radiotracer is present long enough to allow a patient injected at peak treadmill exercise to move to the camera and still be effectively imaged. Feasibility of rest-treadmill exercise ^{18}F flurpiridaz was initially shown in Phase 1 clinical trials (44, 45). A very high target-to-background ratio was noted when ^{18}F flurpiridaz was injected at peak treadmill exercise. Using the relationship between rest-stress contamination and dosing, it was determined that for a same-day rest-exercise protocol, a minimum dose ratio of 3.0 was needed, with a 60-minute waiting time between the 2 injections. For an optimum same-day rest-adenosine stress protocol, on the other hand, a dose ratio of 3 with a 30-minute waiting time between the 2 injections was required (44, 45). These protocols were successfully implemented in the Phase 2 and Phase 3 clinical trials of ^{18}F flurpiridaz.

Peak stress function imaging—Kinetic studies in Phase 1 trials (45) have shown that imaging may begin 2min following injection of ^{18}F flurpiridaz during pharmacological stress. With treadmill exercise protocol, imaging may begin as soon as the patient is moved under the PET imaging device following completion of exercise. Using ^{18}F flurpiridaz, post stress imaging is, therefore, very close to peak stress and has a higher chance of detecting stress induced wall motion abnormalities. This is in contrast with ^{99m}Tc SPECT MPI protocol in which post stress images are obtained 30-45min following stress.

Diagnostic accuracy for detection of CAD—In the Phase 2 trial (41) of ^{18}F flurpiridaz, diagnostic performance of this tracer was compared to ^{99m}Tc SPECT MPI for detection of CAD defined as ≥50% stenosis by invasive coronary angiography (ICA). 143 patients from 21 centers underwent rest-stress PET and ^{99m}Tc SPECT MPI. In 86 patients who underwent ICA, sensitivity of PET was higher than SPECT (78.8% vs. 61.5%, respectively, $p = 0.02$). Specificity was not significantly different (PET: 76.5% vs. SPECT: 73.5%). Receiver-operating characteristic curve area was 0.82 ± 0.05 for PET and 0.70 ± 0.06 for SPECT ($p = 0.04$) (Figure 3). Normalcy rate was 89.7% with PET and 97.4% with SPECT (p = NS). Figure 4 illustrates a patient who underwent ^{99m}Tc labeled SPECT MPI and ^{18}F flurpiridaz MPI who was subsequently found to have normal coronary arteries on invasive coronary angiography. The SPECT MPI was a false positive due to the presence of a reversible inferior wall defect. ^{18}F flurpiridaz MPI showed uniform distribution of activity throughout the myocardium and therefore was truly negative. The patient shown in Figure 5 had a normal SPECT MPI. ^{18}F flurpiridaz MPI, however, showed reversible anterolateral defects that correlated with the presence of significant left circumflex coronary disease on ICA.

Absolute quantitation of myocardial blood flow—The importance of absolute quantitation of myocardial flow, above and beyond relative perfusion imaging, has been well established and is progressively entering routine clinical practice (46) (47) (9). ^{13}N ammonia CFR increases diagnostic sensitivity (48) and has a strong association with prognosis (49) (50). ^{82}Rb MBF and CFR correctly detects 3-vessel CAD (51) and predicts adverse cardiovascular events (29) beyond relative MPI (30) (31). Most importantly, absolute quantitation of MBF with ^{82}Rb is a strong and independent predictor of cardiac

mortality in patients with known or suspected CAD, providing incremental risk stratification over established clinical variables and relative MPI (32).

The elevated extraction fraction of ^{18}F flurpiridaz at different flow rates makes it an optimal candidate for absolute MBF quantitation. In an initial study, Nekolla and associates used a 3-compartmental modeling approach in a pig model for quantitation of MBF with ^{18}F flurpiridaz (39). In this 3-compartment kinetic model, k1 was the extraction from the arterial blood to the interstitium, essentially representing MBF; k2 the reverse diffusion of the radiotracer from the interstitium to the vascular space; and k3 represented the binding of the radiotracer from the interstitium to the cardiomyocyte MC-1. k4, theoretically describing the reverse diffusion of the radiotracer from the cardiomyocyte MC-1 to the interstitium was set at zero given the very high retention rate of ^{18}F flurpiridaz. Given the single-pass extraction fraction was known to be 94%, no correction for flow-dependent extraction was applied. With the use of adenosine stress and LAD constriction, regional flow values ranged from 0.1 – 3.0 mL/min/g. Results of the 3-compartment model fitting were 80% over a 10min and 84% over a 20min acquisition period. There was overall significant agreement between the kinetic modeling and MBF measured by microspheres, with a modest underestimation of MBF using this model leading to a slope=0.84 and r=0.88. The underestimation of MBF was more accentuated in LAD constriction, with a slope=0.61 and r=0.93.

Another simplified method of absolute flow quantitation utilizing ^{18}F flurpiridaz and allowing radiotracer injection outside the PET scanner was proposed in a pig model (52). Here, the authors posited that myocardial retention and standardized uptake values (SUV) based on late uptake could provide estimates of CFR. These represent simplified methods, given radiotracer retention is a model-free approach in which tracer uptake is calibrated with myocardial radiotracer delivery, and given SUV represents myocardial uptake calibrated with the patient's dose and weight. Radioactive microspheres were injected concomitantly to ^{18}F flurpiridaz in the left atrium. Myocardial retention and SUV of ^{18}F flurpiridaz were calculated using the averaged myocardial activity concentration. Myocardial retention was measured by averaging regional myocardial activities at various time-points. This average was subsequently normalized to the area under the blood curve in the 1st 3min after injection. SUVs were also calculated at various time-points at rest and stress. Both showed the best correlation with the 3-compartment kinetic model or microspheres at 5-12min after injection. However, at later intervals of 5-15min, 10-15min and 10-20min after injection, both retention and SUV underestimated MBF. The authors then calculated the ratios of stress and rest values of CFR-retention and CFR-SUV which were then compared to CFR-^{18}F flurpiridaz and CFR-microspheres. For CFR-retention vs. CFR-microspheres, the slope=0.63 and r=0.92 at 5-12min after injection. For CFR-SUV vs. CFR-microspheres, the slope=1.13 and r=0.95 5-12min after injection. At later time points, both CFR-retention and CFR-SUV values had poor concordance with either CFR-^{18}F flurpiridaz or CFR-microspheres. Given the good correlation of CFR-retention and particularly of CFR-SUV following radiotracer injection with measured absolute quantitation methods at 5-12min, and given that SUV measurement does not require tracer input function and hence could be measured even when the radiotracer is injected outside the PET scanner, the authors conclude that this approach would permit combination of flow quantitation with exercise treadmill protocols.

Our group recently completed the first in human absolute quantitation of MBF with ^{18}F flurpiridaz (53). Study patients were participants in the phase II clinical trial of ^{18}F flurpiridaz at the University of California, Los Angeles (UCLA) (41). Analyses were performed in both normal subjects and CAD patients providing MBF data over a wide range of conditions. Our approach does not necessitate compartmental modeling. Dynamic polar maps were obtained and time-activity-curves generated. Quantitative myocardial perfusion was estimated using the tracer uptake kinetics within the first 90 seconds post tracer injection. Within this period, the tracer was assumed to be taken up by the myocardium without significant clearance, and with very few if any labeled metabolites contained in the blood. Since the kinetic data were corrected for partial volume effect, spillover of activities between myocardium and blood pool, and vascular activity, the MBF value obtained corresponded to the blood perfusion value in the myocardium with blood in the vasculature removed. We found that CFR in patients with a low likelihood of CAD and territories supplied by normal coronary arteries was 3.7± 0.39, while CFR was significantly lower in myocardial regions supplied by diseased coronary arteries (1.86± 0.59). Although the first-pass extraction fraction was taken directly from an animal study, its use in our approach gives human MBF values comparable to the commonly accepted values obtained by other methods. Indeed, our results are in a similar range as those measured with other radiotracers such as ^{82}Rb chloride, ^{13}N ammonia and ^{15}O water. Moreover, our results obtained with ^{18}F flurpiridaz do not necessitate a correction such as that often utilized in the case of Rb82 for example (54).

Fluorodihydrorotenone (^{18}F-FDHR)—Rotenone is a neutral lipophilic compound that also binds to complex I in the mitochondrial electron transport chain (55). Rotenone is an inhibitor of MC-I and competitively inhibits the enzyme by competing for binding with ubiquinone. The exact characteristic of fluorodihydrorotenone's binding has not been fully evaluated. Isolated rabbit hearts were perfused and radiotracer kinetics assessed at flow rates ranging from 0.3 – 3.5 mL/min/g of left ventricle. The radioagent was not studied using a microPET imaging system, but rather myocardial extraction, retention and washout were computed from the venous outflow curves with the multiple-indicator technique and spectral analysis. Results were compared to ^{201}Tl and to the vascular reference tracer ^{131}I-albumin. The mean extraction fraction of ^{18}F-FDHR and ^{201}Tl were similar; however the initial extraction fraction of ^{18}F -FDHR declined with flow. Overall, the investigators observed that the myocardial retention was higher and less affected by flow than that of ^{201}Tl, leading to superior correlation with flow 1min and 15min after radiotracer injection. Unfortunately, no followup studies with ^{18}F-FDHR were conducted.

p-Fluorobenzyl triphenyl phosphonium cation (^{18}F-FBnTP)—^{18}F-FBnTP is a lipophilic cation. The delocalized positive charge of the compound allows it to cross the lipid bilayer by passive diffusion and accumulate in cells in a membrane potential-dependent manner. Due to its greater membrane potential, the radiotracer accumulates mainly in the mitochondria (56). The main clearance route is renal. The metabolic stability, uptake kinetics in isolated myocytes and in dog myocardium, as well as the myocardial and whole-body distribution in dogs were analyzed (57). In isolated myocytes, ^{18}F-FBnTP results in rapid accumulation and prolonged retention, reaching 91% of the mean plateau activity after

15min, and 88% of control activity after 60min and 85% after 120min, respectively. Similar results are observed *in vivo*, with the radiotracer reaching a plateau in the left ventricular myocardium within 5min of administration, and a prolonged retention time up to 90min observed. In dogs, the metabolite fraction analyzed by high-performance liquid chromatography of plasma comprises <5% of total activity in blood at 5min, <9% at 10min and gradually increases to 24% at 30min after injection. However, the absolute concentration of metabolites in the blood is very low, around 3% after 20min, due to rapid tissue accumulation of the radiotracer. Whereas blood pool and lung activity decreases over time, leading to favorable uptake ratios to the heart, the ration of heart to liver is 1.2 after 60min. Despite this, high-quality cardiac images are produced with visualization of anatomic details including papillary muscles and atria. Similar radiotracer activity is observed in all quadrants. Whole body distribution of ^{18}F-FBnTP demonstrates that the kidney cortex is the major target organ, followed by the heart and the liver.

In a followup study, the authors investigated the ability of ^{18}F-FBnTP PET vs. ^{99m}Tc-tetrofosmin SPECT to assess the severity of coronary artery stenosis in dogs with various degrees of stenosis in the left anterior descending (LAD) and left circumflex coronary (LCx) arteries in an acute model of ischemia with intact myocardial viability (58). The authors utilized radioactive microspheres as the gold standard to determine true myocardial blood flow and Monastral blue staining to assess the risk area. ^{18}F-FBnTP myocardial regional activity was measured *ex vivo* by direct tissue γ-well counting and *in vivo* by dynamic PET imaging. The LAD or LCx arteries were dissected free 1-2cm from the origin and a cuff occluder placed around the artery. The authors demonstrated that ^{18}F-FBnTP PET was superior to ^{99m}Tc-tetrofosmin SPECT in assessing mild or severe stenosis compared to normal territories, with a flow defect contrast that was 2.7 times greater in favor of ^{18}F-FBnTP. In both stenotic and normal vascular beds, peak ^{18}F-FBnTP activity was obtained within 10-20sec after injection, and a near-plateau concentration observed within the following 10-20sec. This plateau activity was retained throughout the scanning time of up to 60min. The mean risk area by ^{18}F-FBnTP PET was 84% of the true extent measured by Monastral blue-stained cardiac sections. The underestimation of the risk area is far less than that reported for technetium complexes which are typically in the 30% range. Finally, the authors note that in patients with chronic ischemia, either in the setting of repetitive stunning or myocardial infarction, the effect of tissue viability, mitochondrial bioenergetics and membrane potential – the driving force of ^{18}F-FBnTP uptake by the myocardium – were not assessed.

In a similar followup study in rats, the investigators analyzed the ability of ^{18}F-FBnTP to delineate the ischemic area after transient coronary occlusion in rats and assessed the presence of tracer washout and redistribution (59). Rats underwent thoracotomy and a 2min occlusion by suture against a snare of the left coronary artery was conducted at which time the radiotracer was injected, followed by reperfusion which was obtained by release of the snare. 1min prior to sacrifice, the animals underwent repeat occlusion of the left coronary artery by repositioning the snare with concomitant injection of Evans blue dye to determine the ischemic territory. ^{18}F-FBnTP demonstrated stable ischemic defects at all time points (5min, 45min, and 120min) following radiotracer injection and excellent correlation with the

Evans blue dye determined histological ischemic area (R^2=0.94). A comparison was conducted at each time-point with ^{201}Tl which exhibited redistribution and hence absence of significant defect after 120min – a known phenomenon with this SPECT tracer. The lack of redistribution for at least 45min of ^{18}F-FBnTP should permit development of clinically feasible protocols. Interestingly, ^{18}F-FBnTP also detects apoptosis and has a strong negative correlation with the Bax (pro-apoptotic) – to – Bcl-2 (anti-apoptotic) ratio (R^2 = 0.83) and release of the apoptogen cytochrome c (R^2 = 0.92) in breast cancer cells. This additional property is described in detail elsewhere (60).

4-Fluorophenyl triphenyl phosphonium ion (^{18}F-FTPP)—A related lipophilic cationic radiotracer but differing structurally and in electronic charge distribution, 4-fluorophenyl triphenyl phosphonium ion (^{18}F-FTPP), also targets the mitochondria and accumulates in the mitrochondrial matrix due to the relatively high mitochondrial interior membrane potential. ^{18}F-FTPP was evaluated as a potential PET MBF agent (61). Biodistribution studies were performed in normal rats at 5, 30 and 60min and in rabbits before and after occlusion of the LAD accomplished by tightening of a snare around the artery in the setting of thoracotomy. Results were compared with ^{13}N ammonia. Uptake was highest in the kidneys at all time points. Heart uptake was 1.5% of the injected dose per gram. MicroPET imaging demonstrated an initial spike of activity corresponding to blood flow followed by rapid washout and a plateau after 1-2min. After 5min, ratios were 11 for heart/blood, 2 for heart/lung and 5 for heart/liver. After 30min, these ratios were 75, 5 and 8 respectively and remained in a similar range at 60min. Images in the regions of interest and corresponding time-activity curves obtained following LAD occlusion were of similar quality between ^{18}F-FTPP and ^{13}N-ammonia.

Conclusion

For decades, PET MPI was mostly limited to academic research centers and large hospital systems while SPECT MPI remained the default approach in routine clinical practice by which patients underwent cardiac risk stratification and evaluation of stress-inducible myocardial ischemia. The enhanced sensitivity and specificity of PET radiotracers compared to SPECT radiotracers, as well as their inherent attenuation correction and ability to quantitate flow in an absolute manner further increases the value of a PET based approach. The major Achilles heel of routine PET MPI however has been the availability of radiotracers, with current requirement for either onsite or very nearby cyclotrons or costly generators. In this context ^{18}F-based PET radiotracers, taking advantage of the radioisotope's 108min half-life, have garnered significant interest and have been developed by academic centers and biotechnology companies. Of the reported ^{18}F-based PET MPI radiotracers, only ^{18}F flurpiridaz is in advanced clinical evaluation with encouraging results.

Acknowledgments

Funding: ^{18}F flurpiridaz clinical trials have been sponsored by Lantheus Medical Imaging. Lantheus Medical Imaging had no role writing of this manuscript. Dr. Packard is supported by NIH grant T32 HL007895. Dr. Maddahi is supported by a research grant from Lantheus Medical Imaging.

References

1. Dilsizian V, Taillefer R. Journey in evolution of nuclear cardiology: will there be another quantum leap with the F-18-labeled myocardial perfusion tracers? JACC Cardiovasc Imaging. 2012; 5:1269–1284. [PubMed: 23236979]
2. Rischpler C, Park MJ, Fung GS, Javadi M, Tsui BM, Higuchi T. Advances in PET myocardial perfusion imaging: F-18 labeled tracers. Ann Nucl Med. 2012; 26:1–6. [PubMed: 22069195]
3. Nekolla SG, Saraste A. Novel F-18-labeled PET myocardial perfusion tracers: bench to bedside. Curr Cardiol Rep. 2011; 13:145–150. [PubMed: 21207199]
4. Bergmann SR, Fox KA, Rand AL, et al. Quantification of regional myocardial blood flow in vivo with H215O. Circulation. 1984; 70:724–733. [PubMed: 6332687]
5. Garcia, EV.; Galt, JR.; Faber, TL., et al. Principles of nuclear cardiology imaging. In: Dilsizian, Vasken; Narula, Jagat, editors. Atlas of Nuclear Cardiology. 4th edition. Springer Science; 2013. p. 1-53.Chapter 1
6. Bol A, Melin JA, Vanoverschelde JL, et al. Direct comparison of [13N]ammonia and [15O]water estimates of perfusion with quantification of regional myocardial blood flow by microspheres. Circulation. 1993; 87:512–525. [PubMed: 8425298]
7. Kajander SA, Joutsiniemi E, Saraste M, et al. Clinical value of absolute quantification of myocardial perfusion with (15)O-water in coronary artery disease. Circ Cardiovasc Imaging. 2011; 4:678–684. [PubMed: 21926262]
8. Nitzsche EU, Choi Y, Czernin J, et al. Noninvasive quantification of myocardial blood flow in humans. A direct comparison of the [13N]ammonia and the [15O]water techniques. Circulation. 1996; 93:2000–2006. [PubMed: 8640974]
9. Schindler TH, Schelbert HR, Quercioli A, et al. Cardiac PET imaging for the detection and monitoring of coronary artery disease and microvascular health. JACC Cardiovasc Imaging. 2010; 3:623–640. [PubMed: 20541718]
10. Bergmann SR, Hack S, Tewson T, et al. The dependence of accumulation of 13NH3 by myocardium on metabolic factors and its implications for quantitative assessment of perfusion. Circulation. 1980; 61:34–43. [PubMed: 7349940]
11. Schelbert HR, Phelps ME, Huang SC, et al. N-13 ammonia as an indicator of myocardial blood flow. Circulation. 1981; 63:1259–1272. [PubMed: 7226473]
12. Krivokapich J, Huang SC, Phelps ME, et al. Dependence of 13NH3 myocardial extraction and clearance on flow and metabolism. Am J Physiol. 1982; 242:H536–542. [PubMed: 7065268]
13. Tamaki N, Yonekura Y, Senda M, et al. Myocardial positron computed tomography with 13N-ammonia at rest and during exercise. Eur J Nucl Med Mol Imaging. 1985; 11:246–251.
14. Krivokapich J, Smith GT, Huang SC, et al. 13N ammonia myocardial imaging at rest and with exercise in normal volunteers. Quantification of absolute myocardial perfusion with dynamic positron emission tomography. Circulation. 1989; 80:1328–1337. [PubMed: 2805269]
15. Chow BJ, Beanlands RS, Lee A, et al. Treadmill exercise produces larger perfusion defects than dipyridamole stress N-13 ammonia positron emission tomography. J Am Coll Cardiol. 2006; 47:411–416. [PubMed: 16412870]
16. Czernin J, Muller P, Chan S, et al. Influence of age and hemodynamics on myocardial blood flow and flow reserve. Circulation. 1993; 88:62–69. [PubMed: 8319357]
17. Di Carli M, Czernin J, Hoh CK, et al. Relation among stenosis severity, myocardial blood flow, and flow reserve in patients with coronary artery disease. Circulation. 1995; 91:1944–1951. [PubMed: 7895351]
18. Schindler TH, Nitzsche EU, Olschewski M, et al. Chronic inflammation and impaired coronary vasoreactivity in patients with coronary risk factors. Circulation. 2004; 110:1069–1075. [PubMed: 15313940]
19. Prior JO, Quinones MJ, Hernandez-Pampaloni M, et al. Coronary circulatory dysfunction in insulin resistance, impaired glucose tolerance, and type 2 diabetes mellitus. Circulation. 2005; 111:2291–2298. [PubMed: 15851590]

20. Schindler TH, Cardenas J, Prior JO, et al. Relationship between increasing body weight, insulin resistance, inflammation, adipocytokine leptin, and coronary circulatory function. J Am Coll Cardiol. 2006; 47:1188–1195. [PubMed: 16545651]
21. Love WD, Burch GE. A comparison of potassium 42, rubidium 86, and cesium 134 as tracers of potassium in the study of cation metabolism of human erythrocytes in vitro. J Lab Clin Med. 1953; 41:351–362. [PubMed: 13035272]
22. Love WD, Romney RB, Burch GE. A comparison of the distribution of potassium and exchangeable rubidium in the organs of the dog, using rubidium. Circ Res. 1954; 2:112–122. [PubMed: 13141374]
23. Selwyn AP, Allan RM, L'Abbate A, et al. Relation between regional myocardial uptake of rubidium-82 and perfusion: absolute reduction of cation uptake in ischemia. Am J Cardiol. 1982; 50:112–121. [PubMed: 6979917]
24. El Fakhri G, Kardan A, Sitek A, et al. Reproducibility and accuracy of quantitative myocardial blood flow assessment with (82)Rb PET: comparison with (13)N-ammonia PET. J Nucl Med. 2009; 50:1062–1071. [PubMed: 19525467]
25. Naya M, Murthy VL, Taqueti VR, et al. Preserved coronary flow reserve effectively excludes high-risk coronary artery disease on angiography. J Nucl Med. 2014; 55:248–255. [PubMed: 24408896]
26. Goldstein RA, Mullani NA, Marani SK, et al. Myocardial perfusion with rubidium-82. II. Effects of metabolic and pharmacologic interventions. J Nucl Med. 1983; 24:907–915. [PubMed: 6619961]
27. Huang SC, Williams BA, Krivokapich J, et al. Rabbit myocardial 82Rb kinetics and a compartmental model for blood flow estimation. Am J Physiol. 1989; 256:H1156–1164. [PubMed: 2784945]
28. Herrero P, Markham J, Shelton ME, et al. Noninvasive quantification of regional myocardial perfusion with rubidium-82 and positron emission tomography. Exploration of a mathematical model. Circulation. 1990; 82:1377–1386. [PubMed: 2401071]
29. Fukushima K, Javadi MS, Higuchi T, et al. Prediction of short-term cardiovascular events using quantification of global myocardial flow reserve in patients referred for clinical 82Rb PET perfusion imaging. J Nucl Med. 2011; 52:726–732. [PubMed: 21498538]
30. Ziadi MC, Dekemp RA, Williams KA, et al. Impaired myocardial flow reserve on rubidium-82 positron emission tomography imaging predicts adverse outcomes in patients assessed for myocardial ischemia. J Am Coll Cardiol. 2011; 58:740–748. [PubMed: 21816311]
31. Farhad H, Dunet V, Bachelard K, et al. Added prognostic value of myocardial blood flow quantitation in rubidium-82 positron emission tomography imaging. Eur Heart J Cardiovasc Imaging. 2013; 14:1203–1210. [PubMed: 23660750]
32. Murthy VL, Naya M, Foster CR, et al. Improved cardiac risk assessment with noninvasive measures of coronary flow reserve. Circulation. 2011; 124:2215–2224. [PubMed: 22007073]
33. Kim DY, Kim HS, Le UN, et al. Evaluation of a mitochondrial voltage sensor, (18F-fluoropentyl)triphenylphosphonium cation, in a rat myocardial infarction model. J Nucl Med. 2012; 53:1779–1785. [PubMed: 23038748]
34. Kim DY, Kim HJ, Yu KH, et al. Synthesis of [18F]-labeled (2-(2-fluoroethoxy)ethyl)tris(4-methoxyphenyl)phosphonium cation as a potential agent for positron emission tomography myocardial imaging. Nucl Med Biol. 2012; 39:1093–1098. [PubMed: 22575270]
35. Kim DY, Kim HJ, Yu KH, et al. Synthesis of [18F]-labeled (6-fluorohexyl)triphenylphosphonium cation as a potential agent for myocardial imaging using positron emission tomography. Bioconjug Chem. 2012; 23:431–437. [PubMed: 22264022]
36. Kim DY, Kim HJ, Yu KH, et al. Synthesis of [(1)(8)F]-labeled (2-(2-fluoroethoxy)ethyl)triphenylphosphonium cation as a potential agent for myocardial imaging using positron emission tomography. Bioorg Med Chem Lett. 2012; 22:319–322. [PubMed: 22133630]
37. Yalamanchili P, Wexler E, Hayes M, et al. Mechanism of uptake and retention of F-18 BMS-747158-02 in cardiomyocytes: a novel PET myocardial imaging agent. J Nucl Cardiol. 2007; 14:782–788. [PubMed: 18022104]
38. Yu M, Guaraldi MT, Mistry M, et al. BMS-747158-02: a novel PET myocardial perfusion imaging agent. J Nucl Cardiol. 2007; 14:789–798. [PubMed: 18022105]

39. Nekolla SG, Reder S, Saraste A, et al. Evaluation of the novel myocardial perfusion positron-emission tomography tracer 18F-BMS-747158-02: comparison to 13N-ammonia and validation with microspheres in a pig model. Circulation. 2009; 119:2333–2342. [PubMed: 19380625]
40. Sherif HM, Saraste A, Weidl E, et al. Evaluation of a novel (18)F-labeled positron-emission tomography perfusion tracer for the assessment of myocardial infarct size in rats. Circ Cardiovasc Imaging. 2009; 2:77–84. [PubMed: 19808572]
41. Berman DS, Maddahi J, Tamarappoo BK, et al. Phase II safety and clinical comparison with single-photon emission computed tomography myocardial perfusion imaging for detection of coronary artery disease: flurpiridaz F 18 positron emission tomography. J Am Coll Cardiol. 2013; 61:469–477. [PubMed: 23265345]
42. Huisman MC, Higuchi T, Reder S, et al. Initial characterization of an 18F-labeled myocardial perfusion tracer. J Nucl Med. 2008; 49:630–636. [PubMed: 18344426]
43. Maddahi J. Properties of an ideal PET perfusion tracer: new PET tracer cases and data. J Nucl Cardiol. 2012; 19:S30–37. [PubMed: 22259007]
44. Maddahi J, Czernin J, Lazewatsky J, et al. Phase I, first-in-human study of BMS747158, a novel 18F-labeled tracer for myocardial perfusion PET: dosimetry, biodistribution, safety, and imaging characteristics after a single injection at rest. J Nucl Med. 2011; 52:1490–1498. [PubMed: 21849402]
45. Maddahi J, Bengel F, Huang S-C, et al. Phase 1 rest-stress study of F-18 labeled BMS747158 myocardial perfusion PET tracer: Human safety, dosimetry, biodistribution, and myocardial imaging characteristics [abstract]. J Nucl Med. 2009; 50:184. [PubMed: 19164225]
46. Gould KL, Johnson NP, Bateman TM, et al. Anatomic versus physiologic assessment of coronary artery disease. Role of coronary flow reserve, fractional flow reserve, and positron emission tomography imaging in revascularization decision-making. J Am Coll Cardiol. 2013; 62:1639–1653. [PubMed: 23954338]
47. Johnson NP, Gould KL. Integrating noninvasive absolute flow, coronary flow reserve, and ischemic thresholds into a comprehensive map of physiological severity. JACC Cardiovasc Imaging. 2012; 5:430–440. [PubMed: 22498334]
48. Fiechter M, Ghadri JR, Gebhard C, et al. Diagnostic value of 13N-ammonia myocardial perfusion PET: added value of myocardial flow reserve. J Nucl Med. 2012; 53:1230–1234. [PubMed: 22776752]
49. Tio RA, Dabeshlim A, Siebelink HM, et al. Comparison between the prognostic value of left ventricular function and myocardial perfusion reserve in patients with ischemic heart disease. J Nucl Med. 2009; 50:214–219. [PubMed: 19164219]
50. Herzog BA, Husmann L, Valenta I, et al. Long-term prognostic value of 13N-ammonia myocardial perfusion positron emission tomography added value of coronary flow reserve. J Am Coll Cardiol. 2009; 54:150–156. [PubMed: 19573732]
51. Parkash R, deKemp RA, Ruddy TD, et al. Potential utility of rubidium 82 PET quantification in patients with 3-vessel coronary artery disease. J Nucl Cardiol. 2004; 11:440–449. [PubMed: 15295413]
52. Sherif HM, Nekolla SG, Saraste A, et al. Simplified quantification of myocardial flow reserve with flurpiridaz F 18: validation with microspheres in a pig model. J Nucl Med. 2011; 52:617–624. [PubMed: 21441533]
53. Packard RRS, Huang S-C, Dahlbom M, et al. Absolute quantitation of myocardial blood flow in human subjects with or without myocardial ischemia using dynamic F18 flurpiridaz positron emission tomography. J Nucl Med. in revision.
54. Saraste A, Kajander S, Han C, et al. PET: Is myocardial flow quantification a clinical reality? J Nucl Cardiol. 2012; 19:1044–1059. [PubMed: 22733534]
55. Marshall RC, Powers-Risius P, Reutter BW, et al. Kinetic analysis of 18F-fluorodihydrorotenone as a deposited myocardial flow tracer: comparison to 201Tl. J Nucl Med. 2004; 45:1950–1959. [PubMed: 15534068]
56. Madar I, Ravert H, Nelkin B, et al. Characterization of membrane potential-dependent uptake of the novel PET tracer 18F-fluorobenzyl triphenylphosphonium cation. Eur J Nucl Med Mol Imaging. 2007; 34:2057–2065. [PubMed: 17786439]

57. Madar I, Ravert HT, Du Y, et al. Characterization of uptake of the new PET imaging compound 18F-fluorobenzyl triphenyl phosphonium in dog myocardium. J Nucl Med. 2006; 47:1359–1366. [PubMed: 16883017]

58. Madar I, Ravert H, Dipaula A, et al. Assessment of severity of coronary artery stenosis in a canine model using the PET agent 18F-fluorobenzyl triphenyl phosphonium: comparison with 99mTc-tetrofosmin. J Nucl Med. 2007; 48:1021–1030. [PubMed: 17504876]

59. Higuchi T, Fukushima K, Rischpler C, et al. Stable delineation of the ischemic area by the PET perfusion tracer 18F-fluorobenzyl triphenyl phosphonium after transient coronary occlusion. J Nucl Med. 2011; 52:965–969. [PubMed: 21571789]

60. Madar I, Huang Y, Ravert H, et al. Detection and quantification of the evolution dynamics of apoptosis using the PET voltage sensor 18F-fluorobenzyl triphenyl phosphonium. J Nucl Med. 2009; 50:774–780. [PubMed: 19372481]

61. Shoup TM, Elmaleh DR, Brownell AL, et al. Evaluation of (4-[18F]Fluorophenyl)triphenylphosphonium ion. A potential myocardial blood flow agent for PET. Mol Imaging Biol. 2011; 13:511–517. [PubMed: 20563755]

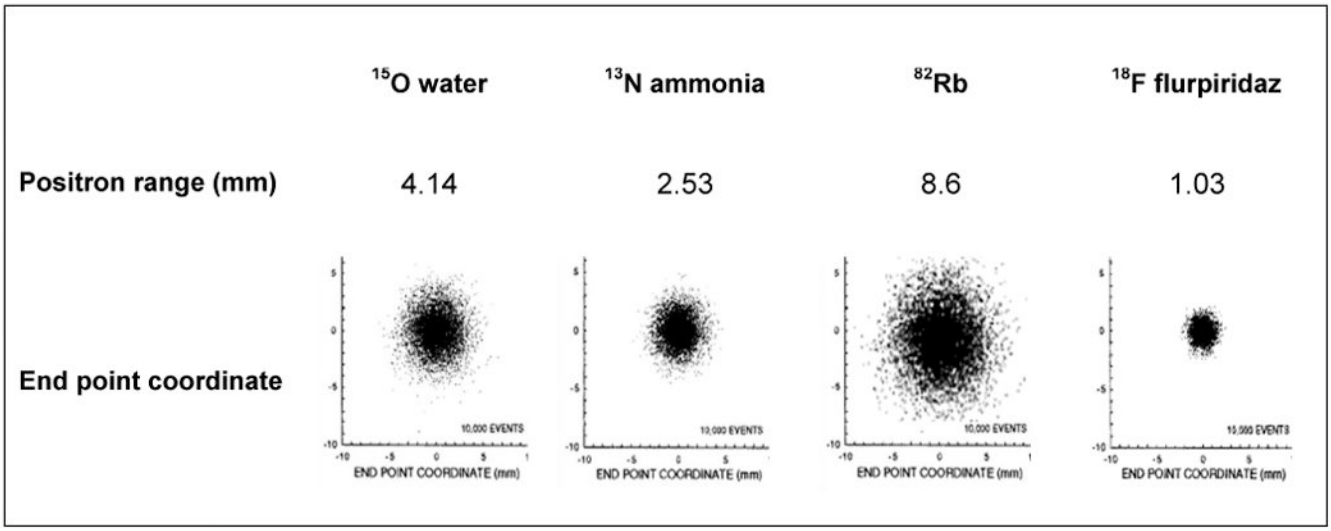

Figure 1.

Positron range and end point coordinates are shown for various myocardial perfusion PET tracers. The higher the energy of the emitted positron, the longer it travels away from the source before annihilation and the worse the resolution of the imaged target. In this figure, end point coordinates are similar to point source images obtained from a given PET tracer.

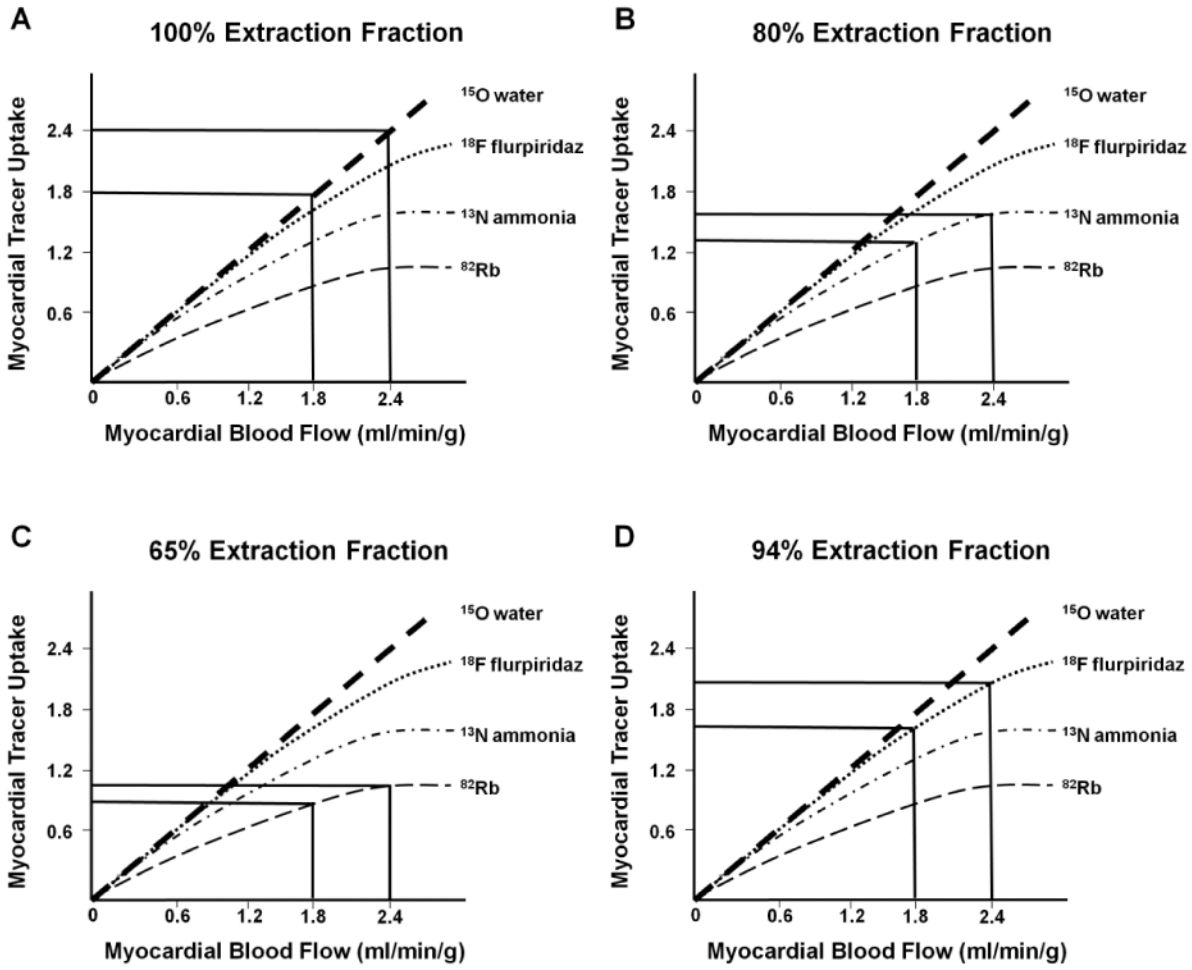

Figure 2.

Conceptual effect of radiotracer extraction fraction on detection of myocardial perfusion defect severity. Myocardial uptake of various PET tracers (y-axes) are shown when myocardial blood flow (x-axes) increases by a greater increment in a vascular bed supplied by a normal coronary artery versus a lower increment in the myocardial region supplied by a narrowed coronary artery. The differences in myocardial uptake of various tracers are illustrated for ^{15}O water (Figures 2a), ^{13}N ammonia (Figures 2b), ^{82}RB (Figure 2c) and ^{18}F flurpiridaz (Figures 2d). *See text for detailed explanation*

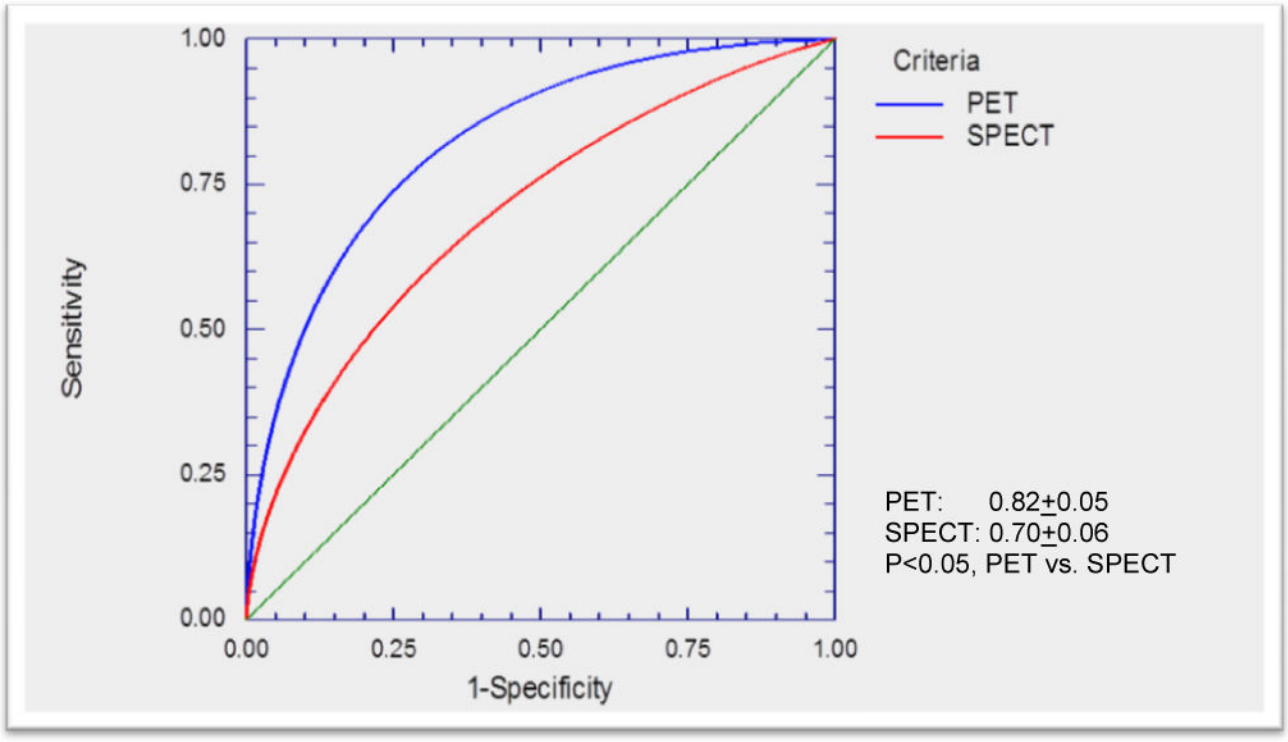

Figure 3.

Receiver Operating Curves (ROC) for ^{18}F flurpiridaz (blue) and ^{99m}Tc labeled SPECT (red) for detection of coronary artery disease in Phase 2 ^{18}F flurpiridaz multicenter study. The area under the ROC curve for ^{18}F flurpiridaz was significantly better than that of ^{99m}Tc labeled SPECT ($p<0.05$).

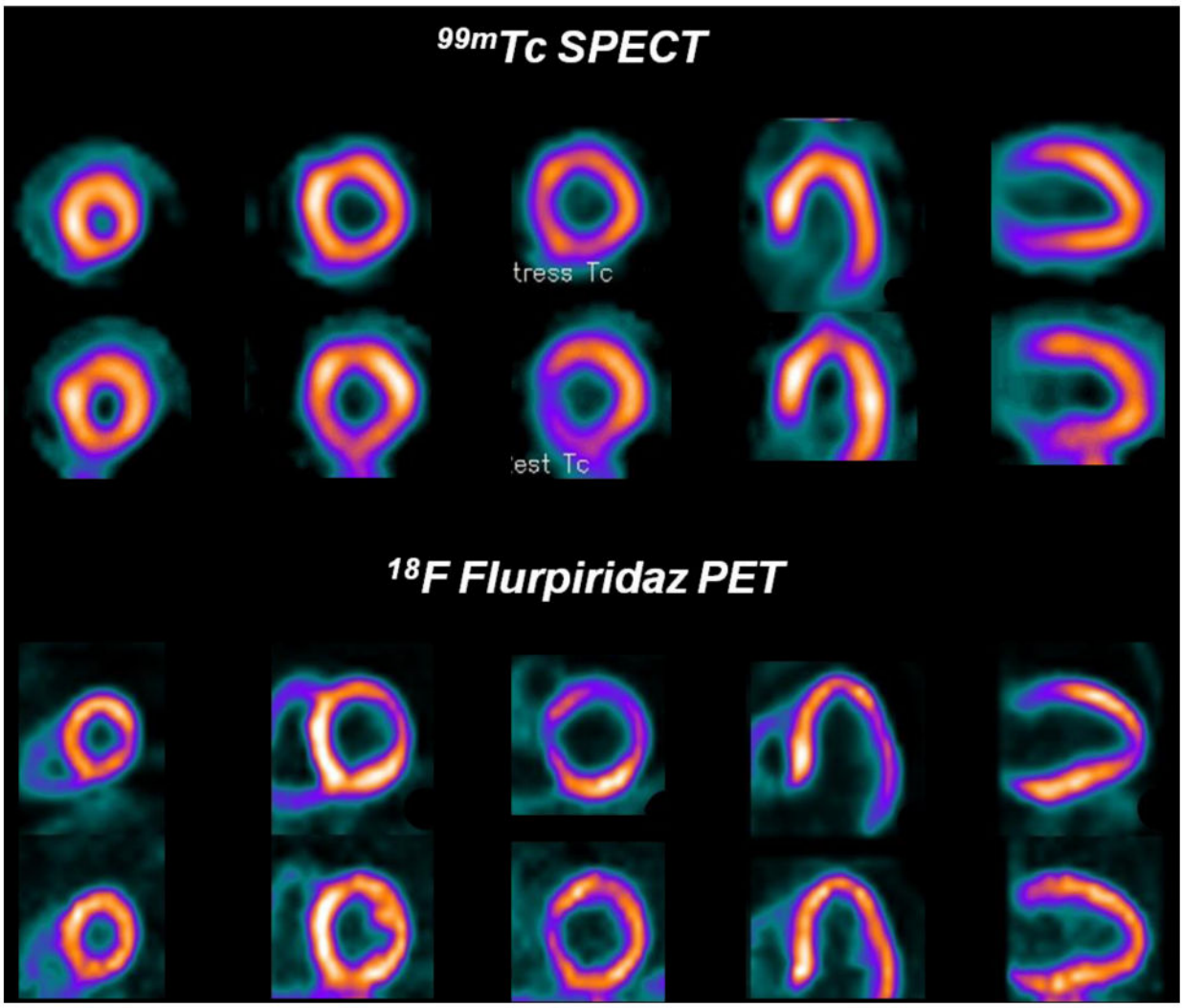

Figure 4.
^{99m}Tc SPECT images (upper rows) and flurpiridaz F 18 PET images (lower rows) from a patient with normal coronary arteries. A false positive reversible inferior defect is present on the ^{99m}Tc SPECT images due to shifting soft-tissue attenuation. The flurpiridaz F 18 PET study, however, provided superior image quality and was normal.

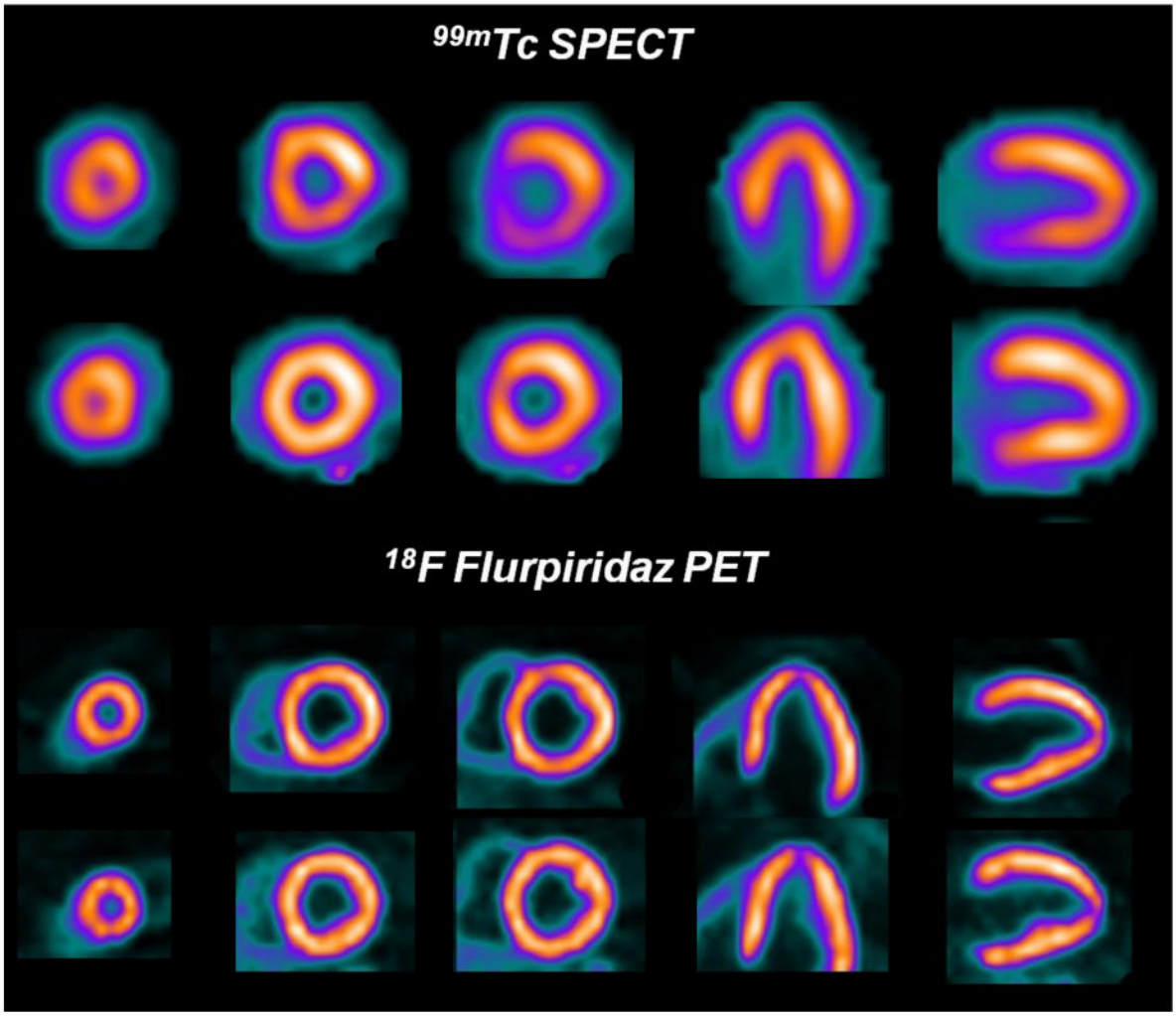

Figure 5.
^{99m}Tc SPECT and ^{18}F flurpiridaz PET images in a patient with significant disease in the left circumflex coronary artery. The overall quality of the ^{18}F flurpiridaz PET images (lower rows) was superior to the ^{99m}Tc SPECT images (upper rows). ^{18}F flurpiridaz PET images showed reversible anterolateral wall defects in the distribution of the diseased left circumflex coronary artery, but the ^{99m}Tc SPECT images were normal.

Table 1

Characteristics of various cardiac PET perfusion tracers.

	^{15}O water	^{13}N ammonia	^{82}Rb	^{18}F flurpiridaz
Half life (minutes)	2.06	9.96	1.25	109
Production	On-site cyclotron	On-site or nearby cyclotron	Generator	Regional cyclotron
Positron range (mm)	4.14	2.53	8.6	1.03
Image resolution	Intermediate	Intermediate-high	Lowest	Highest
Myocardial extraction fraction	100%	80%	65%	94%
Perfusion defect contrast	Intermediate*	Intermediate	Lowest	Highest
Pharmacological stress imaging protocol	Feasible	Feasible	Feasible	Feasible
Treadmill exercise Imaging protocol	Not feasible	Feasible but not practical	Not feasible	Feasible

*Theoretically 100% myocardial extraction fraction of ^{15}O water should result in the highest perfusion defect contrast. However, poor myocardial-to-background ratio reduces defect contrast.